Spectral Properties of Multicarrier Signals under Broadband Signal Alignment

Roberto López-Valcarce, *Senior Member, IEEE*

***Abstract*— Broadband signal alignment (BSA) is a recently proposed scheme that introduces frequency-domain repetition coding in multicarrier transmission. Combined with canonical correlation analysis (CCA) at the multiantenna receiver, this approach provides robustness against strong interference. We derive an analytical expression for the power spectral density (PSD) of BSA-encoded multicarrier signals and show that the original scheme generally degrades out-of-band sidelobes. We then propose a modified BSA approach that unlocks additional degrees of freedom to be exploited for sidelobe reduction while preserving the interference resilience of the original scheme. Our analysis reveals that the frequency-domain data repetition pattern is a critical design parameter, as it significantly impacts both spectral characteristics and error-rate performance.**

***Index Terms*— Multicarrier modulation, underlay communication, OFDM, power spectral density, broadband signal alignment.**

I. Introduction

Orthogonal Frequency-Division Multiplexing (OFDM) has become the modulation of choice in modern multicarrier systems due to its robustness against multipath and good matching with multiple-input multiple-output (MIMO) techniques. Recently, a novel scheme termed Broadband Signal Alignment (BSA) has been proposed in [1] for single-input multiple-output (SIMO) systems to make OFDM resilient against strong and unpredictable interference, such as that encountered in adversarial settings or underlay wireless communication scenarios. In the latter, secondary users share the spectrum with more powerful primary users without coordination, and must accept any interference caused by the primary network [2]. At the transmitter, BSA hinges on repetition coding across subcarriers, whereas at the receiver, the use of multiple antennas together with the judicious application of Canonical Correlation Analysis (CCA) tools [3] allows data recovery with very short training preambles even under powerful interference. It was also shown in [1] via testbed experiments that carrier frequency offset (CFO) correction and frame alignment are feasible under BSA precoding.

Robustness of BSA to strong interference comes at the price of reduced spectral efficiency: if all data symbols are to be protected, then each one of them must be transmitted on at least two different subcarriers, so that the spectral efficiency is at most half that of a conventional OFDM system using the same subcarrier spacing and total number of active subcarriers. Moreover, it is well known that OFDM modulation suffers from large sidelobes resulting in increased out-of-band radiation (OBR). This further compromises spectral efficiency, as sidelobe reduction techniques for OFDM consume additional time or frequency resources [4]–[7]. In underlay scenarios, higher OBR increases the *interference temperature* [2], degrading the performance of both primary and secondary receivers. Given that BSA introduces subcarrier correlation, it is important to understand the effect of frequency repetition coding on the transmit signal's power spectral density (PSD). In this sense, the contributions of this letter are as follows:

- We leverage the analysis from [8] to derive an analytical expression for the PSD. Notably, sidelobes increase under BSA by an amount that depends on the frequency repetition pattern.
- We modify the original BSA scheme by applying complex-valued scalings to data repetitions. It is shown that the same CCA techniques can still be used at the receiver to estimate the data; however, the complex scalars provide additional degrees of freedom. We present a design to exploit these for sidelobe reduction without sacrificing additional time or frequency resources.
- The performance of the proposed design is evaluated through numerical examples in terms of OBR reduction, error rate, and peak-to-average-power ratio (PAPR). Results show the importance of selecting an appropriate data repetition pattern in the frequency domain.

BSA was originally designed based on OFDM for sufficiently slow-varying multipath settings [1], as the channel response must remain approximately constant within a frame duration. Novel multicarrier-like waveforms have been recently proposed as better alternatives to OFDM under fast fading [9]: these schemes remain vulnerable to interference, and thus the applicability of BSA concepts to fast-fading resilient waveforms is a topic of interest for future work.

Notation: Vectors (resp. matrices) are denoted by boldface lowercase (resp. uppercase) symbols. $\boldsymbol{A}^T$, $\boldsymbol{A}^H$, $\|\boldsymbol{A}\|_F$, $\operatorname{tr}\boldsymbol{A}$, $\boldsymbol{A}[i,j]$ denote transpose, conjugate transpose, Frobenius norm, trace, and (i,j)-th element of $\boldsymbol{A}$. $\boldsymbol{I}_n$ and $\mathbf{1}_n$ denote the $n\times n$ identity matrix and $n\times 1$ vector of all ones. The i-th column of the identity matrix with appropriate dimension is denoted by $\boldsymbol{e}_i$. The Euclidean norm of $\boldsymbol{v}$ is denoted as $\|\boldsymbol{v}\|$. $\operatorname{diag}(\cdot)$ and $\operatorname{blkdiag}(\cdot)$ denote diagonal and block-diagonal matrices, resp. The Kronecker delta and product are denoted as δ_m and $\otimes$ resp., and $\mathbb{E}\{\cdot\}$ is the expectation operator.

II. Signal model

We consider a single-user communication system, with a single-antenna transmitter and a multiple-antenna receiver. The transmitter sends a multicarrier signal generated with an IFFT

The author is with atlanTTic (Research Center in Telecommunications), Universidade de Vigo, 36310 Vigo, Spain. Email: valcarce@gts.uvigo.es
Work funded by MCIN/AEI/10.13039/501100011033/ FEDER "A way of making Europe" under project MAYTE (PID2022-136512OB-C22). Funding for open access charge: Universidade de Vigo/CISUG.

This article has been accepted for publication in IEEE Communications Letters. This is the author's version which has not been fully edited and content may change prior to final publication. Citation information: DOI 10.1109/LCOMM.2026.3660876

of size N, with $\mathcal{K} = \{k_1, k_2, \ldots, k_K\}$ the set of indices of active subcarriers. Let $x_k^{(\ell)}$ be the data modulated on the k-th subcarrier of the ℓ-th OFDM symbol, collected in the vector $\boldsymbol{x}_\ell = \begin{bmatrix} x_{k_1}^{(\ell)} & x_{k_2}^{(\ell)} & \cdots & x_{k_K}^{(\ell)} \end{bmatrix}^T \in \mathbb{C}^K$. Then the baseband samples of the multicarrier signal are given by

$$s[n] = \sum_{\ell=-\infty}^{\infty} \sum_{k\in\mathcal{K}} x_k^{(\ell)} h[n-\ell L] \mathrm{e}^{\jmath\frac{2\pi}{N}k(n-\ell L)}, \qquad (1)$$

where $L \geq N$ is the hop size in samples, and $h[n]$ is the shaping pulse, with Fourier transform $H(\mathrm{e}^{\jmath\omega}) = \sum_{n=-\infty}^{\infty} h[n]\mathrm{e}^{-\jmath\omega n}$. Depending of the choice of pulse $h[n]$, (1) encompasses different multicarrier variants including cyclic prefix (CP), zero padding (ZP) and windowing (W) OFDM [8]. We focus on CP-OFDM with rectangular pulses, for which $h[n] = 1$ for $0 \leq n \leq L-1$ and zero otherwise, and the CP length is $N_{\mathrm{cp}} = L - N$. However, our analysis can be readily extended to other pulse types. The samples $s[n]$ in (1) are fed to a digital-to-analog converter (DAC) with sampling rate $f_s = \frac{1}{T_s}$ to obtain the baseband continuous-time signal:

$$s(t) = \sum_{n=-\infty}^{\infty} s[n] h_{\mathrm{I}}(t - nT_s), \qquad (2)$$

where $h_{\mathrm{I}}(t)$ is the impulse response of the DAC interpolation filter, with Fourier transform $H_{\mathrm{I}}(f) = \int_{-\infty}^{\infty} h_{\mathrm{I}}(t)\mathrm{e}^{-\jmath 2\pi f t}\mathrm{d}t$. The subcarrier spacing is then $\Delta_f = \frac{1}{NT_s}$.

The following is a useful particular case of [8, Th. 1].

Lemma 1: Assume that the process $\{\boldsymbol{x}_\ell\}$ is zero-mean and satisfies $\mathbb{E}\{\boldsymbol{x}_\ell \boldsymbol{x}_{\ell'}^T\} = \mathbf{0}$, $\mathbb{E}\{\boldsymbol{x}_\ell \boldsymbol{x}_{\ell'}^H\} = \delta_{\ell-\ell'}\boldsymbol{C}$ for all (ℓ, ℓ'). Let $\phi_k(f) \triangleq \frac{1}{LT_s} H_{\mathrm{I}}(f) H^*\left(\mathrm{e}^{\jmath 2\pi(f-k\Delta_f)T_s}\right)$, and also

$$\boldsymbol{\phi}(f) \triangleq \begin{bmatrix} \phi_{k_1}(f) & \phi_{k_2}(f) & \cdots & \phi_{k_K}(f) \end{bmatrix}^T. \qquad (3)$$

Then, the PSD of the baseband signal $s(t)$ in (2) is given by

$$S_s(f) = \boldsymbol{\phi}^H(f)\boldsymbol{C}\boldsymbol{\phi}(f). \qquad (4)$$

III. Broadband Signal Alignment

BSA [1] is based on a frequency repetition coding scheme as follows. For the ℓ-th OFDM symbol, $D \leq K$ data points, collected in the data vector $\boldsymbol{d}_\ell \in \mathbb{C}^D$, are mapped to the K available subcarriers, *i.e.,* to the modulating vector $\boldsymbol{x}_\ell \in \mathbb{C}^K$, according to a specific repetition pattern:

$$\boldsymbol{x}_\ell = \boldsymbol{\Pi}\boldsymbol{E}_0\boldsymbol{d}_\ell, \qquad (5)$$

where:

- $\boldsymbol{E}_0 \in \mathbb{C}^{K\times D}$ is a block-diagonal *repetition matrix:*

$$\boldsymbol{E}_0 \triangleq \mathrm{blkdiag}\begin{pmatrix} \mathbf{1}_{R_1} & \mathbf{1}_{R_2} & \cdots & \mathbf{1}_{R_C} & \boldsymbol{I}_{D-C} \end{pmatrix}. \qquad (6)$$

  Thus, the first R_1 entries of $\boldsymbol{E}_0\boldsymbol{d}_\ell$ are repetitions of the first entry of $\boldsymbol{d}_\ell$, the next R_2 rows are repetitions of the second entry of $\boldsymbol{d}_\ell$, etc. Note that the last $D - C$ entries of $\boldsymbol{d}_\ell$ are not repeated. After repetitions, the number of used subcarriers is $K = D - C + \sum_{c=1}^{C} R_c$.
- $\boldsymbol{\Pi} \in \mathbb{C}^{K\times K}$ is a permutation matrix mapping the rows of $\boldsymbol{E}_0\boldsymbol{d}_\ell$ to the desired subcarrier positions in $\boldsymbol{x}_\ell$. Thus, different choices of $\boldsymbol{\Pi}$ result in different repetition arrangements. Although the selection of $\boldsymbol{\Pi}$ was not discussed in [1], we shall show that it has a significant influence in the spectral properties of the transmit signal.

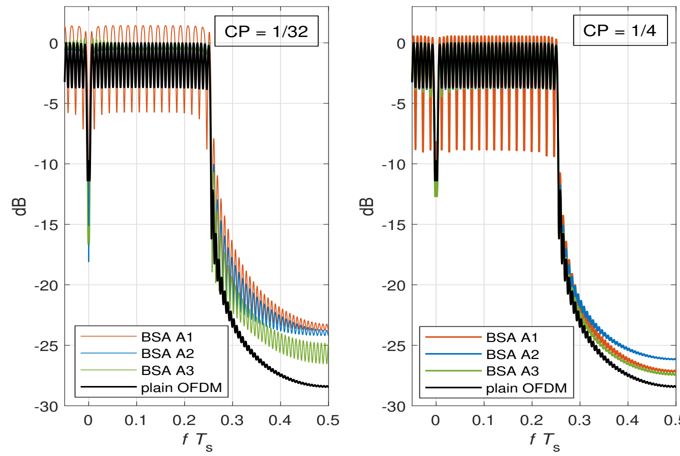

(a) (b)

Fig. 1. PSD under different BSA arrangements. $N = 128$, $K = 64$.

Data are assumed zero mean, unit-variance i.i.d., *i.e.,* $\boldsymbol{d}_\ell[i]$, $\boldsymbol{d}_{\ell'}[i']$ are statistically independent for $(i', \ell') \neq (i, \ell)$. It is also assumed that $\mathbb{E}\{(\boldsymbol{d}_\ell[i])^2\} = 0$ for all (i, ℓ), which will hold for most quadrature amplitude modulation (QAM) constellations, but not for, *e.g.,* binary phase-shift keying (BPSK). Then the process $\{\boldsymbol{x}_\ell\}$ satisfies the conditions of Lemma 1 with $\boldsymbol{C} = \boldsymbol{\Pi}\boldsymbol{E}_0\boldsymbol{E}_0^H\boldsymbol{\Pi}^H$. Thus, under broadband signal alignment, the PSD of the multicarrier signal $s(t)$ is given by

$$S_s(f) = \left\|\boldsymbol{E}_0^H\boldsymbol{\Pi}^H\boldsymbol{\phi}(f)\right\|^2 = \sum_{c=1}^{D}\left|\sum_{k\in\mathcal{R}_c}\phi_k(f)\right|^2, \qquad (7)$$

where $\mathcal{R}_c \subset \mathcal{K}$ is the set of subcarrier indices to which the data point in the c-th entry of $\boldsymbol{d}_\ell$ is copied. Note that $|\mathcal{R}_c| = R_c$ for $c = 1, \ldots, C$, whereas $|\mathcal{R}_c| = 1$ for $c = C+1, \ldots, D$.

As an example, consider a rectangularly-pulsed CP-OFDM system with $N = 128$ and $K = 64$ active subcarriers symmetrically located around the dc subcarrier, which is turned off, and $D = K/2$. Thus, $\mathcal{K} = \{-32, \ldots, -1, +1, \ldots, +32\}$. Each data symbol is repeated once, so $C = D$ and $R_c = 2$, $c = 1, \ldots, C$. We shall refer to subcarriers carrying the same data as *twin subcarriers.* We consider three different arrangements for data repetitions:

A1) $\boldsymbol{\Pi} = \boldsymbol{I}_K$, so that $\boldsymbol{\Pi}\boldsymbol{E}_0 = \boldsymbol{E}_0 = \boldsymbol{I}_{K/2} \otimes \mathbf{1}_2$. Thus, twin subcarriers are always contiguous.

A2) $\boldsymbol{\Pi}\boldsymbol{E}_0 = [\boldsymbol{I}_{K/2}\ \boldsymbol{I}_{K/2}]^T$: twin subcarriers are separated by $(K/2+1)\Delta_f$ Hz.

A3) $\boldsymbol{\Pi}\boldsymbol{E}_0 = [\boldsymbol{I}_{K/2}\ \boldsymbol{J}_{K/2}]^T$, where $\boldsymbol{J}_n \in \mathbb{C}^{n\times n}$ is the reversal matrix with ones in the antidiagonal and zeros elsewhere. The separation between twin subcarriers varies between $K\Delta_f$ (at the passband edges) and $2\Delta_f$ Hz (at the passband center).

The corresponding PSDs, all normalized to the same transmit power, are shown in Fig. 1, for the cases of a short and long CP ($\frac{N_{\mathrm{cp}}}{N} = \frac{1}{32}$ and $\frac{1}{4}$ resp.). The DAC filter $H_{\mathrm{I}}(f)$ is assumed ideal lowpass with cutoff frequency $\frac{1}{2T_s}$. The PSD for the CP-OFDM system with the same K subcarriers active but

This article has been accepted for publication in IEEE Communications Letters. This is the author's version which has not been fully edited and content may change prior to final publication. Citation information: DOI 10.1109/LCOMM.2026.3660876

without repetition encoding is also shown as reference. All three arrangements A1-A3 result in increased sidelobes with respect to the baseline system, more so for short CP, with A3 resulting in least degradation for both CP lengths

IV. Generalized BSA

A. Receive processing: Original BSA

The BSA decoding scheme proposed in [1] is outlined next. This scheme requires the use of $M \geq 2$ antennas at the receiver to provide robustness to strong interference. BSA operation is *frame-based* [1], where each frame is composed of P consecutive OFDM symbols. A block-fading model is adopted, meaning that the channels can be assumed to be invariant over the duration of a frame. Thus, let the q-th frame comprise the OFDM symbols qP, $qP+1$,…,$qP+P-1$, and define the corresponding frame matrices before and after repetition coding, respectively, as

$$\boldsymbol{D}_q = \begin{bmatrix} \boldsymbol{d}_{qP} & \boldsymbol{d}_{qP+1} & \cdots & \boldsymbol{d}_{qP+P-1} \end{bmatrix} \in \mathbb{C}^{D\times P}, \quad (8)$$

$$\boldsymbol{X}_q = \begin{bmatrix} \boldsymbol{x}_{qP} & \boldsymbol{x}_{qP+1} & \cdots & \boldsymbol{x}_{qP+P-1} \end{bmatrix} \in \mathbb{C}^{K\times P}, \quad (9)$$

so that, from (5), one has $\boldsymbol{X}_q = \boldsymbol{\Pi}\boldsymbol{E}_0\boldsymbol{D}_q$. After CP removal and FFT processing, the received q-th frame at the m-th antenna, $m \in \{1,\ldots,M\}$, can be written as

$$\boldsymbol{Z}_{m,q} = \boldsymbol{\Lambda}_{m,q}\boldsymbol{X}_q + \boldsymbol{\Gamma}_{m,q}\widetilde{\boldsymbol{X}}_q + \boldsymbol{N}_{m,q}, \quad (10)$$

where $\widetilde{\boldsymbol{X}}_q \in \mathbb{C}^{K\times P}$ represents the interference, $\boldsymbol{N}_{m,q} \in \mathbb{C}^{K\times P}$ is the additive white Gaussian noise at the m-th antenna, and $\boldsymbol{\Lambda}_{m,q}$, $\boldsymbol{\Gamma}_{m,q} \in \mathbb{C}^{K\times K}$ are diagonal matrices containing the frequency response coefficients of the channels from the signal and interference transmitters, respectively, to the m-th receive antenna. These channels are assumed to be invariant over the frame duration. Since the received frames are processed sequentially, we drop the frame index q for conciseness. Using $\boldsymbol{X} = \boldsymbol{\Pi}\boldsymbol{E}_0\boldsymbol{D}$, it follows from (10) that

$$\hat{\boldsymbol{Z}}_m \triangleq \boldsymbol{\Pi}^H\boldsymbol{Z}_m = \hat{\boldsymbol{\Lambda}}_m\boldsymbol{E}_0\boldsymbol{D} + \boldsymbol{\Pi}^H\boldsymbol{\Gamma}_m\widetilde{\boldsymbol{X}} + \boldsymbol{\Pi}^H\boldsymbol{N}_m, \quad (11)$$

where $\hat{\boldsymbol{\Lambda}}_m \triangleq \boldsymbol{\Pi}^H\boldsymbol{\Lambda}_m\boldsymbol{\Pi} \in \mathbb{C}^{K\times K}$ remains diagonal.

Consider the *signal views* $\boldsymbol{Y}_k \in \mathbb{C}^{M\times P}$, constructed as

$$\boldsymbol{Y}_k = \begin{bmatrix} \boldsymbol{e}_k^H\hat{\boldsymbol{Z}}_1 \\ \vdots \\ \boldsymbol{e}_k^H\hat{\boldsymbol{Z}}_M \end{bmatrix}, \quad k \in \{1,\ldots,K\}. \quad (12)$$

It is seen that the signal component of $\boldsymbol{Y}_k$ has rank 1:

$$\begin{bmatrix} \boldsymbol{e}_k^H\hat{\boldsymbol{\Lambda}}_1\boldsymbol{E}_0\boldsymbol{D} \\ \vdots \\ \boldsymbol{e}_k^H\hat{\boldsymbol{\Lambda}}_M\boldsymbol{E}_0\boldsymbol{D} \end{bmatrix} = \begin{bmatrix} \hat{\boldsymbol{\Lambda}}_1[k,k] \\ \vdots \\ \hat{\boldsymbol{\Lambda}}_M[k,k] \end{bmatrix} \boldsymbol{e}_k^H\boldsymbol{E}_0\boldsymbol{D}. \quad (13)$$

Let $\bar{R}_0 = 0$ and $\bar{R}_c = R_1 + \cdots + R_c$, $c \in \{1,\ldots,C\}$. Then, for all k such that $\bar{R}_{c-1} < k \leq \bar{R}_c$, it holds that $\boldsymbol{e}_k^H\boldsymbol{E}_0 = \boldsymbol{e}_c^H$. Consequently, the right singular vector of (13) is identical for all k within this range, and equal to $\boldsymbol{e}_c^H\boldsymbol{D}$, *i.e.,* the c-th row of $\boldsymbol{D}$. This property is exploited in [1] by leveraging the maximum variance (MAXVAR) formulation of CCA to estimate $\boldsymbol{e}_c^H\boldsymbol{D}$, up to a scaling factor, from the signal views $\{\boldsymbol{Y}_k,\, \bar{R}_{c-1} < k \leq \bar{R}_c\}$. The scaling ambiguity can then be resolved, *e.g.,* by solving a linear least squares (LS) problem, provided a short preamble is embedded in $\boldsymbol{D}$ [1].

B. Proposed design

Consider now a modification of the original BSA scheme in which the transmit frame is computed as $\boldsymbol{X} = \boldsymbol{\Pi}\boldsymbol{E}\boldsymbol{D}$, with

$$\boldsymbol{E} \triangleq \operatorname{blkdiag}\begin{pmatrix} \boldsymbol{u}_1 & \boldsymbol{u}_2 & \cdots & \boldsymbol{u}_C & \boldsymbol{I}_{D-C} \end{pmatrix} \in \mathbb{C}^{K\times D}, \quad (14)$$

and where $\boldsymbol{u}_c \in \mathbb{C}^{R_c}$, $c = 1,\ldots,C$. This generalizes (6) in the sense that different data repetitions may be scaled by different constants; if $\boldsymbol{u}_c = \boldsymbol{1}_{R_c}$ for all c, then $\boldsymbol{E} = \boldsymbol{E}_0$ and the original scheme from [1] is recovered. Note that, since $\boldsymbol{u}_c = \operatorname{diag}(\boldsymbol{u}_c)\boldsymbol{1}_{R_c}$, (14) can be written as $\boldsymbol{E} = \boldsymbol{\Delta}\boldsymbol{E}_0$, where $\boldsymbol{\Delta} \in \mathbb{C}^{K\times K}$ is diagonal and given by

$$\boldsymbol{\Delta} \triangleq \operatorname{diag}\left(\begin{bmatrix} \boldsymbol{u}_1^T & \boldsymbol{u}_2^T & \cdots & \boldsymbol{u}_C^T & \boldsymbol{1}_{D-C}^T \end{bmatrix}^T\right). \quad (15)$$

Thus, the signal component of $\boldsymbol{Y}_k$ retains the structure of (13) after replacing $\hat{\boldsymbol{\Lambda}}_m$ with $\hat{\boldsymbol{\Lambda}}_m\boldsymbol{\Delta}$, which remains diagonal. Essentially, the terms $\{\boldsymbol{u}_c\}$ are absorbed into the channel coefficients, and the MAXVAR approach can still be applied at the receiver. However, these terms now offer additional degrees of freedom that can be exploited for features such as sidelobe reduction. Now, the PSD of the baseband signal is still given by (4) with $\boldsymbol{C} = \boldsymbol{\Pi}\boldsymbol{E}\boldsymbol{E}^H\boldsymbol{\Pi}^H$. The OBR is defined as the integral of the PSD over some frequency range $\mathcal{W} \subset \mathbb{R}$:

$$P_{\mathcal{W}} \triangleq \int_{\mathcal{W}} S_s(f)\mathrm{d}f = \operatorname{tr}\{\boldsymbol{E}^H\boldsymbol{A}\boldsymbol{E}\}, \quad (16)$$

$$\boldsymbol{A} \triangleq \boldsymbol{\Pi}^H\left(\int_{\mathcal{W}} \boldsymbol{\phi}(f)\boldsymbol{\phi}^H(f)\mathrm{d}f\right)\boldsymbol{\Pi}. \quad (17)$$

Note that $\mathcal{W}$ is a user-selectable parameter, which allows for subband-specific definition of OBR. Using (14), (16) becomes

$$P_{\mathcal{W}} = \sum_{c=1}^{C}\boldsymbol{u}_c^H\boldsymbol{A}_c\boldsymbol{u}_c + \sum_{k=K-D+C+1}^{K}\boldsymbol{e}_k^H\boldsymbol{A}\boldsymbol{e}_k, \quad (18)$$

where $\boldsymbol{A}_c = \boldsymbol{A}[\bar{R}_{c-1}+1 : \bar{R}_c,\, \bar{R}_{c-1}+1 : \bar{R}_c]$ is a diagonal subblock of $\boldsymbol{A}$. The second term on the right-hand side of (18) is due to non-repeated data, whereas the first term can be optimized in terms of $\{\boldsymbol{u}_c\}$. To avoid trivial solutions in which some data are not transmitted, we impose a norm constraint on each of these vectors, formulating the proposed design as

$$\min_{\{\boldsymbol{u}_c\}} \sum_{c=1}^{C}\boldsymbol{u}_c^H\boldsymbol{A}_c\boldsymbol{u}_c \quad \text{s. to} \quad \boldsymbol{u}_c^H\boldsymbol{u}_c = R_c,\; 1 \leq c \leq C. \quad (19)$$

Note that the matrices $\{\boldsymbol{A}_c\}$ in (19) only depend on modulation parameters and the repetition arrangement, and hence (19) can be solved offline. Clearly, (19) decouples into C independent problems: for $c = 1,\ldots,C$, solve $\min_{\boldsymbol{u}_c}\boldsymbol{u}_c^H\boldsymbol{A}_c\boldsymbol{u}_c$ s. to $\boldsymbol{u}_c^H\boldsymbol{u}_c = R_c$. The solution is such that, for $c = 1,\ldots,C$, $\boldsymbol{u}_c$ is the least eigenvector of $\boldsymbol{A}_c$, scaled so that $\|\boldsymbol{u}_c\| = \sqrt{R_c}$.

Note from (17) that the proposed design is for a given permutation matrix $\boldsymbol{\Pi}$. Although it would make sense to minimize $P_{\mathcal{W}}$ in terms of $\boldsymbol{\Pi}$, this would result in a difficult combinatorial problem. Observe, however, that after substituting $\boldsymbol{E}$ for $\boldsymbol{E}_0$ in (7), the PSD can be written as

$$S_s(f) = \sum_{c=1}^{D}\left|\boldsymbol{u}_c^H\boldsymbol{\phi}_c(f)\right|^2, \quad (20)$$

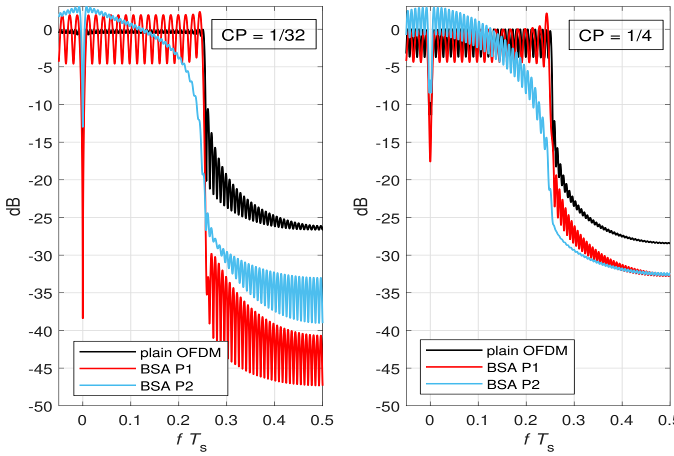

Fig. 2. Sidelobe reduction with the proposed design. $N = 128$, $K = 64$.

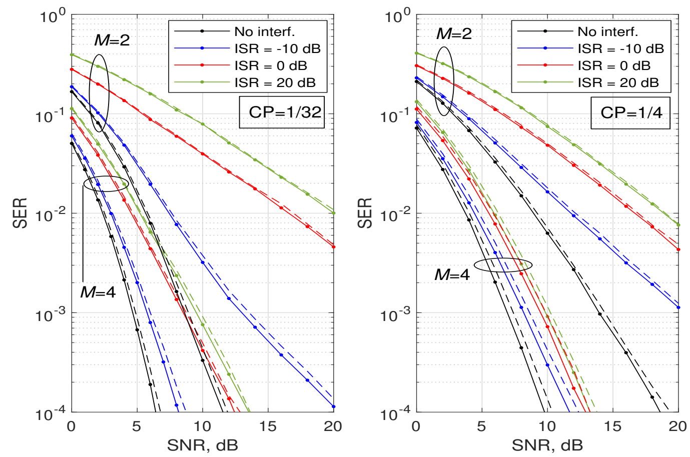

Fig. 3. SER performance of BSA schemes A1 (solid) and P1 (dashed) under QPSK modulation. $N = 128$, $K = 64$, $P = 100$.

where $\boldsymbol{\phi}_c(f) \in \mathbb{C}^{R_c}$ comprises the subcarrier responses $\{\phi_k(f),\, k \in \mathcal{R}_c\}$, and with the convention $\boldsymbol{u}_c = 1 \in \mathbb{R}$ for $C{+}1 \le c \le D$. From (20), it is clear that for $\boldsymbol{u}_c$ to be effective toward sidelobe reduction, the responses $\{\phi_k(f),\, k \in \mathcal{R}_c\}$ should have some overlap in frequency. This means that the subcarriers carrying the scaled repetitions of the same data should not be too far from each other.

In terms of online complexity, at the transmitter the proposed method requires $\bar{R}_C \le K$ additional complex multiplications per OFDM symbol with respect to the original BSA scheme. Notably, no modifications are required at the receiver, as the scalings are treated as part of the unknown effective channel, which also preserves the feasibility of CFO correction and frame alignment.

TABLE I
OBR INCREASE WITH RESPECT TO UNCODED REFERENCE (dB)

BSA Scheme	A1	A2	A3	P1	P2	P3
CP $= 1/32$	2.7	1.2	0.3	-15.6	-10.9	-1.4
CP $= 1/4$	1.0	1.2	0.4	-4.6	-7.7	-1.1

V. Numerical Results

Consider the same scenario as in Fig. 1 (rectangular pulses, $N = 128$, $K = 64$ active subcarriers, $C = D$, $R_c = 2$ $\forall c$). The OBR region is taken as $\mathcal{W} = \{\frac{f_s}{4} + \frac{\Delta_f}{2} \le |f| \le \frac{f_s}{2}\}$. Table I reports the OBR increase in this setting (with respect to the reference CP-OFDM scheme with K active subcarriers and no repetition coding) for the original BSA scheme under arrangements A1, A2 and A3, and for the proposed design (19), termed P1, P2 and P3, so that Pi uses the same permutation matrix $\boldsymbol{\Pi}$ as Ai. Note that A3, which provides maximal separation of twin subcarriers near the passband edges, yields the lowest OBR degradation among the tested arrangements of the original BSA scheme, for both CP lengths considered. Nevertheless, the proposed design results in OBR *improvement,* with a reduction of 15.6 dB (short CP) and of 7.7 dB (long CP), using arrangements P1 and P2, respectively; Fig. 2 shows the corresponding PSDs. It is seen that P1 results in sharp PSD edges and a uniform distribution of power within the passband, whereas under P2 the PSD presents a tapered shape: with this arrangement, subcarriers near the passband edges are significantly scaled down, whereas their corresponding twins located well within the passband are scaled up. As will be seen shortly, this has implications in terms of symbol error rate (SER). The PSD under P3 is not shown for brevity, as it is very close to that of plain OFDM. The fact that P3 is not very effective for OBR reduction agrees with our previous intuition regarding twin subcarrier overlap.

To evaluate the SER performance of BSA, we consider an exponential power delay profile for the block-fading channel. The time-domain channel taps for the m-th receive antenna are synthesized as $c_m[n] = \tilde{c}_m[n] e^{-\frac{n}{2\delta N_{\rm cp}}}$, $0 \le n \le N_{\rm cp} - 1$, with $\tilde{c}_m[n]$ i.i.d. realizations of a circularly symmetric complex Gaussian random variable. The same model is used for the desired and interference channels, which are then normalized so that $\|\boldsymbol{\Lambda}_m\|_F^2 = \|\boldsymbol{\Gamma}_m\|_F^2 = K$ for all m. The signal of interest is quadrature phase shift-keying (QPSK)-modulated with variance σ_d^2, whereas the entries of the interference and noise terms, $\widetilde{\boldsymbol{X}}$ and $\boldsymbol{N}_m$, are i.i.d. circular Gaussian with variances σ_i^2 and σ_n^2, respectively. Accordingly, the SNR and interference-to-signal ratio (ISR) are respectively defined as SNR $\triangleq \frac{\sigma_d^2}{\sigma_n^2}$ and ISR $\triangleq \frac{\sigma_i^2}{\sigma_d^2}$. Frames have length $P = 100$, and a different channel realization with $\delta = 0.1$ is generated for each frame. The MAXVAR approach is applied, with scaling ambiguities resolved via LS estimation based on the first column of each frame $\boldsymbol{D}_q$, assumed known at the receiver.

Results for arrangements A1 and P1 with rectangular pulses are shown in Fig. 3 for both CP lengths, and for $M \in \{2, 4\}$ receive antennas. Although P1 presents a slightly degraded SER with respect to A1, the difference is not significant. The robustness of these arrangements to interference is quite remarkable, especially as the number of receive antennas is increased: at an SER of 10^{-3}, and with $M = 4$ antennas, the effect of an interferer with ISR $= 20$ dB is equivalent to a 5- and 3-dB degradation in SNR for short and long CPs, respectively. With $M = 2$ antennas the system remains operational; however, the sensitivity to interference is substantially larger.

This article has been accepted for publication in IEEE Communications Letters. This is the author's version which has not been fully edited and content may change prior to final publication. Citation information: DOI 10.1109/LCOMM.2026.3660876

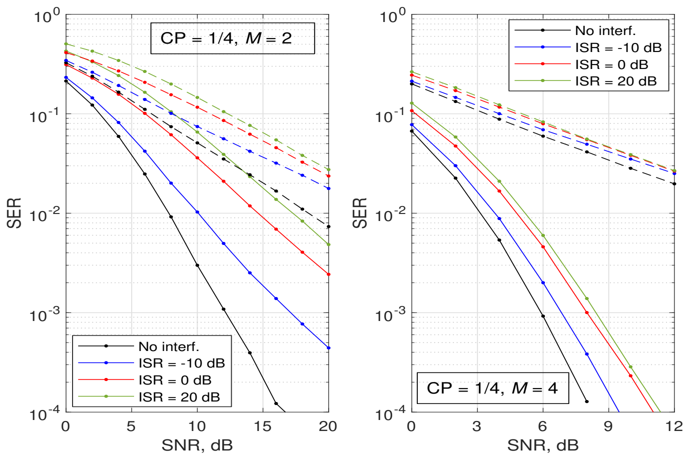

Fig. 4. SER performance of BSA schemes A2 (solid) and P2 (dashed) under QPSK modulation. $N = 128$, $K = 64$, long CP.

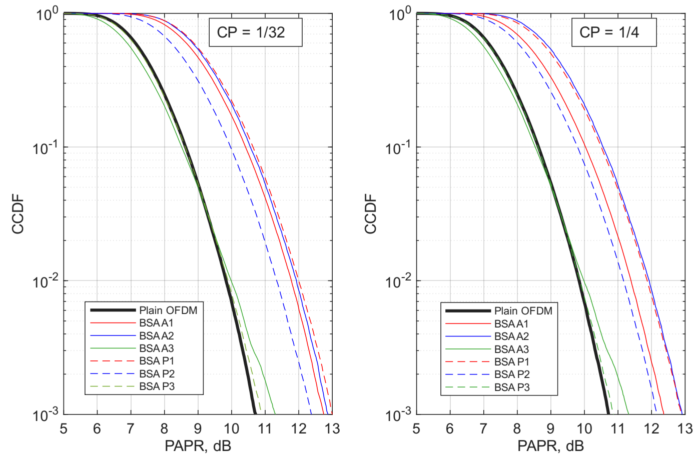

Fig. 5. CCDF of PAPR. $N = 128$, $K = 64$.

The SER for arrangements A2 and P2 is shown in Fig. 4 for the long CP case only. Although not shown for brevity, analogous conclusions can be drawn for the short CP case; additionally, the SER of A3 was very similar to that of A2 for both CP lengths. It is seen that A2 achieves even lower SER values than A1; in contrast, the SER performance of P2 is considerably worse. The reason is that, under P2, the weights for each subcarrier of a given twin pair are heavily unbalanced, resulting in a diversity loss. Although this solution does substantially reduce PSD sidelobes, see Fig. 2, the penalty in terms of error rate is excessive. In this sense, arrangement P1 presents a much better tradeoff between sidelobe reduction and symbol error rate. This can be attributed to the fact that with contiguous twin subcarriers, OBR reduction is primarily achieved by tuning their relative phase without significant magnitude imbalance, thereby preserving diversity. This suggests that, in general, data repetitions should be mapped to proximal subcarriers, as this is beneficial for both sidelobe suppression and SER performance.

High PAPR reduces power amplifier efficiency, making it a critical multicarrier signal parameter [10]. The PAPR of BSA waveforms is shown in Fig. 5 in terms of its complementary cumulative distribution function (CCDF). Interestingly, all tested BSA arrangements degrade the PAPR by 1.3–2 dB relative to the baseline CP-OFDM waveform, except for A3 and P3, which remain close to this baseline. The PAPR degradation of BSA constitutes a justifiable trade-off for the high robustness of these waveforms to interference, which is not enjoyed by conventional CP-OFDM.

In summary, among arrangements A1–A3 of the original BSA scheme, A3 exhibits the lowest sidelobe increase while maintaining favorable PAPR and SER performance. Regarding the proposed designs P1–P3 for sidelobe reduction, P1 emerges as the preferred arrangement; it provides good OBR behavior without an SER penalty and maintains a PAPR similar to that of A1. Notably, while both A1 and P1 exhibit worse PAPR than conventional CP-OFDM, P1 offers the most robust overall trade-off.

VI. Conclusions

Our analysis of BSA-encoded multicarrier signals has shown that inter-carrier correlation introduced by these schemes tends to increase undesirable PSD sidelobes. The proposed modified BSA approach unlocks additional degrees of freedom that can be leveraged for sidelobe reduction. In both cases, the choice of frequency-domain data repetition pattern is of paramount importance.

Our experiments focused on the case where each data symbol is repeated once – the minimal configuration to protect transmission against interference. While the PSD sidelobes of the original BSA scheme experience further regrowth with additional data repetitions, the proposed modification gains more degrees of freedom as repetitions increase, resulting in significantly sharper power spectra.

References

[1] S. Peppas, N. Razavi, and N. D. Sidiropoulos, "Broadband signal alignment for interference resilient multicarrier communication," *IEEE Wireless Commun. Lett.*, vol. 14, no. 4, pp. 974–978, Apr. 2025.

[2] A. Goldsmith, S. A. Jafar, I. Maric, and S. Srinivasa, "Breaking spectrum gridlock with cognitive radios: An information theoretic perspective," *Proc. IEEE*, vol. 97, no. 5, pp. 894–914, May 2009.

[3] J. R. Kettenring, "Canonical analysis of several sets of variables," *Biometrika*, vol. 58, no. 3, pp. 433–451, 1971.

[4] X. Huang, J. A. Zhang, and Y. J. Guo, "Out-of-band emission reduction and a unified framework for precoded OFDM," *IEEE Commun. Mag.*, vol. 53, no. 6, pp. 151–159, Jun. 2015.

[5] L. Díez, J. A. Cortés, F. J. Cañete, E. Martos-Naya, and S. Iranzo, "A generalized spectral shaping method for OFDM signals," *IEEE Trans. Commun.*, vol. 67, no. 5, pp. 3540–3551, 2019.

[6] R. Kumar, K. Hussain, and R. López-Valcarce, "Mask-compliant orthogonal precoding for spectrally efficient OFDM," *IEEE Trans. Commun.*, vol. 69, no. 3, pp. 1990–2001, 2021.

[7] M.-F. Tang and B. Su, "Joint window and filter optimization for new waveforms in multicarrier systems," *EURASIP J. Adv. Signal Process.*, vol. 2018, no. 1, pp. 63–82, Oct. 2018.

[8] R. López-Valcarce, "General form of the power spectral density of multicarrier signals," *IEEE Commun. Lett.*, vol. 26, no. 8, pp. 1755–1759, Aug. 2022.

[9] H. S. Rou *et al.*, "From orthogonal time-frequency space to affine frequency-division multiplexing," *IEEE Signal Process. Mag.*, vol. 41, no. 5, pp. 71–86, Sep. 2024.

[10] Y. Rahmatallah and S. Mohan, "Peak-to-average power ratio reduction in OFDM systems: A survey and taxonomy," *IEEE Commun. Surveys Tuts.*, vol. 15, no. 4, pp. 1567–1592, 2013.